Bright colloidal quantum dot light-emitting diodes enabled by efficient chlorination

Xiyan Li, Yong-Biao Zhao, Fengjia Fan, Larissa Levina, Min Liu, Rafael Quintero-Bermudez, Xiwen Gong, Li Na Quan, James Fan, Zhenyu Yang, Sjoerd Hoogland, Oleksandr Voznyy, Zheng-Hong Lu, and Edward H. Sargent

Bright Colloidal Quantum Dot Light-Emitting Diodes Enabled by Efficient Chlorination

Xiyan Li[1]†, Yong-Biao Zhao[1,2]†, Fengjia Fan[1,3]*, Larissa Levina[1], Min Liu[1,4], Rafael Quintero-Bermudez[1], Xiwen Gong[1], Li Na Quan[1], James Fan[1], Zhenyu Yang[1], Sjoerd Hoogland[1], Oleksandr Voznyy[1]*, Zheng-Hong Lu[2]* and Edward H. Sargent[1]*

[1]Department of Electrical and Computer Engineering, University of Toronto, 35 St George Street, Toronto, Ontario M5S 1A4, Canada.

[2]Department of Materials Science and Engineering, University of Toronto, 184 College Street, Toronto, Ontario M5S 3E4, Canada.

[3]Current Address: CAS Key Laboratory of Microscale Magnetic Resonance and Department of Modern Physics, University of Science and Technology of China (USTC), Hefei 230026, China

[4]Current Address: Institute of Super-microstructure and Ultrafast Process in Advanced Materials, School of Physics and Electronics, Central South University, 932 South Lushan Road, Changsha, Hunan 410083, P. R. China.

* ted.sargent@utoronto.ca, zhenghong.lu@utoronto.ca, o.voznyy@utoronto.ca, ffj@ustc.edu.cn

†These authors contributed equally to this work.

Abstract

The external quantum efficiencies (EQEs) of state-of-the-art colloidal quantum dot light-emitting diodes (QLEDs) are now approaching the limit set by the out-coupling efficiency. However, the brightness of these devices is curtailed by the use of poorly conducting emitting layers, a consequence of present-day reliance on long-chain organic capping ligands. Here, we report how conductive and passivating halides can be implemented in Zn chalcogenide-shelled colloidal quantum dots (CQDs) to enable high-brightness green QLEDs. We use a surface management reagent, thionyl chloride ($SOCl_2$), to chlorinate the carboxylic group of oleic acid and graft the CQD surface with passivating chloride anions. This results in devices with an improved mobility which retain high EQE in the high injection current region and also feature a reduced turn-on voltage of 2.5V. The treated QLEDs operate with a brightness of 460,000 cd m^{-2}, significantly exceeding that of all previously-reported solution-processed LEDs.

Introduction

Light-emitting diodes (LEDs) provide superior contrast over liquid-crystal displays (LCDs) that rely on backlit panels. LEDs based on colloidal quantum dots (QLEDs) provide improved color purity and wavelength tunability compared to organic LEDs[1,2]. For these reasons, continuous efforts have been devoted to improving QLED performance toward the goal of enhanced display and lighting solutions[3-8].

Impressive peak external quantum efficiencies (EQEs) of 12%[9], 16.5%,[10] and 20%[4] have been achieved in blue, green and red QLEDs, respectively. Instead of employing a single CQD monolayer[11], most recent architectures employ several dot layers, with the dots capped using organic ligands that reduce current leakage and suppress exciton quenching at the interfaces with charge ~~transfer~~ transport layers. These organic ligands also provide excellent

passivation that achieves high EQE at low currents; however, because of the ligands' insulating nature, the EQE typically deteriorates at higher brightness[4,12,13]. Replacing long insulating organic ligands with conductive, passivating inorganic ligands has long been pursued to increase charge carrier mobility. This has worked well in the adjacent fields of CQD photovoltaics and field-effect transistor devices[14], with advances coming from halides[15,16], pseudo-halides[17], and metal complexes[18].

To fabricate efficient and bright QLEDs, it is imperative to combine excellent transport with optimized excitonic confinement[19,20]. This can be achieved by growing a passivating and confining shell that prevents exciton dissociation in conductive CQD solids and maintains efficient radiative recombination. The ZnS shell provides symmetric conduction and valence band offsets for the CdSe core, better confining the excitons and balancing the electron and hole mobilities[10,21].

However, a complete exchange with short, transport-compatible inorganic ligands, after which the quantum efficiency can be well maintained, has yet to be developed for ZnS-shelled CQDs[22-27]. Previously-explored ligand exchange approaches have employed anion replacement reactions (Figure 1)[17,18,28]. The driving force of this class of reaction arises from the difference in ligand binding energies before and after the exchange and is therefore significantly determined by the composition of the surface of the CQD[18]. Because of the distinct surface chemistry and large size of ZnS-shelled CQDs, it is challenging to implement ligand exchange through the anion replacement strategy.

For these reasons, QLEDs with simultaneously conductive and bright emitting layers have yet to be demonstrated. Here we developed a robust place exchange strategy, one that instead employs a chlorination reagent ($SOCl_2$, Figure 1), that chlorinates and removes oleic acid ligands and then grafts conductive chloride ligands onto the CQD surface. The driving force for the chlorination reaction, which originates from the capacity of $SOCl_2$ to react with

the carboxylic group of oleic acid, is sufficient to exchange ZnS-shelled CQDs and retain the desired excitonic confinement.

The ligand exchange thereby facilitates charge carrier transport, balancing the spatial distribution of electrons and holes, and thus reducing Auger recombination losses. The photoluminescence quantum yield (PLQY) of the resulting films remains high thanks to the sufficient retention of excitonic confinement.

Results and Discussion

Material synthesis and photophysical properties ~~characterization~~

To achieve efficient QLEDs, we first sought to maximize the PLQY value in CQD solid films. We tested two kinds of CQDs with type-I excitonic confinement: gradient-alloyed CdSeZnS core-shell (C-S) and CdSeZnS-ZnS core-shell-shell (C-S-S) CQDs. The doubly-shelled CQDs here are obtained by growing an additional ZnS shell on the former (see Methods for synthesis details)[29,30]. The sizes of the C-S and C-S-S CQDs, measured using transmission electron microscopy (TEM) images, are 6 nm and 12 nm, respectively, indicating a ZnS shell thickness of 3 nm (Figure 2a and S1a). The blue shift of PL peak (514 nm, Figure S2) indicates a degree of interfacial alloying. The reduced linewidth (FWHM 26 nm) reveals that the alloying process introduced a composition gradient that decreases the inhomogeneity among CQDs.

The PLQY of the C-S-S CQD solution (75%) is not dramatically different from that of C-S CQD solution (70%), consistent with the slightly longer PL lifetime (21 vs. 17 ns) (Figure S3). However, the difference in PLQY is increased when these same CQDs are deposited onto glass substrates. The dramatic drop in PLQY (from 70% to 45%) and shortening in PL decay lifetime in C-S CQD films are attributed to exciton dissociation and trap recombination assisted by Förster resonance energy transfer (FRET) (Figure S4, Table

S1)[21,31]. The extra ZnS shell reduces exciton migration and mitigates PL quenching, preserving high PLQY (63%) and long PL decay lifetime in films (Figure S5).

Efficient chlorination of CQD films

Next we sought to improve the conductivity of the C-S-S CQD films by replacing the insulating long-chain organic ligands with short and conductive halides[32]. Published solution-phase inorganic ligand exchanges[17] failed to provide stable colloids for ZnS shelled CQDs, we ascribe this to strong Zn-to-oleic acid binding and large CQD size after shelling (Figure S6). We focused therefore on developing a solid-state in-place exchange, an approach that provides increased flexibility in the choice of reactive species for ligand exchange. However, we found that conventional approach based on quaternary ammonium halides could not quantitatively remove the organic ligands[16,33,34]. The CQD films following exchange remained soluble in nonpolar solvents, and a strong C-H signal from oleic acid was detected (Figure S7). Chlorotrimethylsilane and propyltrichlorosilane were recently introduced as alternative treatments capable of replacing the organic ligands on the surface of CdSe-based dots with chloride anions[22,23]. However, in prior publications, these exchanges quenched the PL dramatically in solid films. This may be due to excessive shell etching caused by hydrogen chloride (a product of reaction between chlorolsilanes and trace amounts of moisture[35]), precluding their use in QLEDs.

We reasoned that a more efficient chlorination reagent widely used in organic synthetic chemistry, $SOCl_2$[35,36], which is compact in size and capable of reacting with the carboxylic group of oleic acid, could readily penetrate through the films and potentially remove oleic acid even if applied at low concentration. The concentration (0.014 M, see SI) was much lower than that required of tetrabutylammonium chloride (0.14 M, Figure S6, S7)[17] and propyltrichlorosilane (0.5 M) used in previous reports[23]. This would reduce the generation

of hydrogen chloride and circumvent excessive etching of the shell (see Methods for experimental details). This reaction yields CQDs passivated by chloride anions, and free acyl chloride and sulfur dioxide (Figure 1), which are readily removed during the subsequent washing step.

TEM images of the C-S-S CQDs after efficient chlorination, hereafter referred to as C-S-S-Cl (Figure 2b), reveal that the inter-dot distance is shortened after the chlorination (from ~13.5 nm to ~11 nm, Figure 2c). This agrees well with the Fourier-transform infrared spectroscopy (FTIR) spectra (Figure 2d). The characteristic signals attributed to oleic acid, *i.e.* $C–H_x$ stretching signals at 2,922 cm^{-1} and 2,852 cm^{-1}, and O=CO− vibrations at 1,545 cm^{-1} and 1,403 cm^{-1} are eliminated in exchanged films[23]. X-ray photoelectron spectra (Figure S8) further confirm that the CQDs surface is grafted with chloride atomic ligands (Cl 2p, 199.5 eV) whereas the carboxyl groups (C 1s, at 289.2 eV) are removed[37], supporting the reaction scheme presented in Figure 1.

More importantly, the PLQY is maintained (60±2%) after chlorination and no red-shift in PL wavelength is observed (Figure S9a), indicating that the excitons remain well confined. Furthermore, the PL decay dynamics of C-S-S-Cl CQDs remain unchanged when the ZnO/ITO instead of glass substrates are used (Figure S5), showing that CQDs do not become charged[38]. In contrast, even in C-S CQD films on a glass substrate, a significant PLQY decrease (from 45% to 30%) accompanied by a 6 nm red-shift is observed following chlorination exchange (Figure S9b, Table S1). This suggests that FRET-assisted trapping and exciton dissociation become more severe after the exchange.

Device fabrication and characterization

To ascertain whether these bright C-S-S-Cl films show improved transport properties, we fabricated devices with electron-only and hole-only injection, allowing us to measure current density-bias (*J-V)* characteristics (Figure 3a) for each type of carrier independently.

After chlorination-based place-exchange, both the electron and hole currents increased. By fitting the *J-V* curve using space-charge limited current (SCLC) model (Figure S10-S12)[39], we further confirmed that the mobility in the C-S-S-Cl film also increased (Table S2, see fitting details in Supporting Information). Electron and hole currents are more balanced at high bias in both devices (Figure 3a), also observed in previous reports[9,10,25]. We propose that the hopping transport mobility in disordered semiconductors depends strongly on injection level[40] because the density of transport-associated states varies with depth relative to the bandedge[41]. In the case of CQDs, this site energy disorder is dominated by CQD size dispersity; moreover, the conduction band and valence band dispersions are not necessarily the same[42] resulting in unbalanced mobilities at low injection levels. This disorder-induced imbalance can be suppressed at high bias as electron and hole mobilities are enhanced each to a different extent.

Encouraged by the above results, we fabricated C-S-S and C-S-S-Cl CQDs based QLEDs using an inverted device structure[43]. The cross-sectional SEM image, together with the energy diagram of different layers of the C-S-S-Cl QLED, ~~is~~ are illustrated in Figure 3b and 3c. Solution-processed ZnO nanoparticles (35 nm, Figure S13) and thermally evaporated 4,4′-bis(N-carbazolyl)-1,1′-biphenyl (CBP, 55 nm) were used as electron and hole transporting layers (ETL and HTL, the electron affinity and ionization potential were obtained according to references[44,45]), respectively. The thickness of the emissive CQDs layer was 45-50 nm (4-5 layers of QDs). Atomic force microscope (AFM) images confirm that all the layers were pinhole free (Figure S13 and S14), and the root mean squared roughness of the C-S-S-Cl layer on ZnO film is 3.2 nm, which is slightly higher than that of the C-S-S layer (2.2 nm, see supporting information for UPS data (Figure S15, S16)).

The chloride exchange results in a substantial performance improvement over the pristine C-S-S CQD devices. As a result of the improved mobility, the C-S-S-Cl QLED shows higher current densities at given biases throughout the range measured. The turn-on voltage - defined where the brightness reaches 1 cd m^{-2} - is decreased from 3.5 to 2.5 V (Figure 3d,

Table S3). The turn-on voltage of the control device is lower than the value reported recently (~5.2 V) using similar C-S-S CQD, indicating that the control devices are properly optimized[21]. The driving bias to achieve a benchmark luminance of 1,000 cd m^{-2} was also reduced from 4.9 to 3.9 V. The lowering in bias is helpful to mitigate quantum-confined Stark effect (QCSE), a fact that also contributes to the higher EQE in C-S-S-Cl devices at a given brightness[2].

We observed that EQE increases with increasing the bias up to 7.5 V in both devices, as observed in previous reports[7,21,27]. This can be qualitatively understood by considering recombination $R(n)$ in QLED, which consists of three components: trap-assisted nonradiative Shockley-Read-Hall (An), radiative (Bn^2) and Auger (Cn^3) recombination (A, B and C are the related coefficients)[46]. These components show linear, quadratic and cubic dependence on the carrier concentration n (Equation 1), respectively. As a result, recombination at lowest bias is dominated by trap state recombination, at medium bias by radiative recombination, and at high bias by Auger recombination:

$$R(n) = An + Bn^2 + Cn^3 \qquad (1)$$

To achieve high brightness, it is essential to maintain a high EQE at even higher bias and therefore higher current density. Similar to typical QLED devices reported previously, EQE roll-off becomes significant in the C-S-S QLED as the injected current density exceeds 350 mA cm^{-2} (Figure 4a). In contrast, there is no obvious EQE roll-off up to 1,000 mA cm^{-2} in the C-S-S-Cl QLEDs (Figure 4a). Similarly, the EQE starts to roll off at 85,000 cd m^{-2} in the C-S-S QLED, but remains nearly constant in the C-S-S-Cl QLED up to its maximum luminance of 460,000 cd m^{-2} (Figure 4b).

In prior reports, EQE roll-off has been attributed to three possible causes: Joule heating, QCSE[2,14], and Auger recombination[47]. We observed a slight red-shift in the electroluminescence peak in C-S-S devices at a bias of 16 V (Figure 5b), while it is less obvious in C-S-S-Cl devices (Figure 5a), indicating that reduced Joule heating in Cl^-

passivated devices may contribute to the improved maximum brightness. The QCSE effect was excluded as the main cause since EQE roll-off in C-S-S-Cl QLEDs takes place at a much higher bias than in the control devices with identical confining potential within each CQD (Figure 4c). We therefore conclude that the reduced Auger recombination - its ratio lowered due to the increased mobility and a more balanced injection in the new devices - is the main cause of the reduced EQE roll-off in C-S-S-Cl devices.

Device modeling

This hypothesis is supported by more detailed optoelectronic device modeling (Figure 6). A positive effect of increased mobility on reducing Auger recombination losses (see Methods for simulation details) is observed. Simulation results indicate that due to relatively high injection barriers (0.2-0.3 eV), electron and hole concentrations are depleted near the ETL and HTL, respectively, and accumulate at the opposite side of the device (Figure 6a, 6b, and Figure 3c). An improvement in mobility by an order of magnitude results in a more balanced distribution of electrons and holes throughout the thickness of the active layer (Figure 6b). In the low-conductivity case, most charge carriers recombine near the edges, with a major portion lost through Auger recombination. In contrast, with higher mobility, radiative recombination occurs throughout the entire thickness of the layer. Higher mobility leads to a slightly increased trap recombination (SRH recombination in the plot), as this can now compete more efficiently with radiative recombination. The radiative-to-Auger recombination ratio has been improved so that a higher internal quantum efficiency (IQE) (Figure 6c and 6d) can be obtained.

In our C-S-S-Cl device, an EQE of ~6 % was obtained at a high current injection current density of 1,000 mA cm^{-2}, providing improved high-current performance compared to the best-reported QLEDs (Figure 4a, Table S4). As a result, a maximum brightness of

460,000 cd m^{-2} is demonstrated in C-S-S-Cl QLEDs (Figure 3d). This is the highest value reported in an LED employing solution-processed emitting layers (Table S4 and S5)[43,48].

Conclusion

We developed an efficient chlorination that efficiently replaces organic ligands with inorganic single-atomic-layer surface ligands. When we combine the efficient chlorination with judiciously-engineered excitonic confinement, we obtained CQD films with high conductivity and quantum efficiency simultaneously. This facilitates charge carrier injection and mitigates the accumulation of electrons and holes near the ETL and HTL. Auger recombination was therefore suppressed at high injection current densities. As a result, the turn-on voltage of chlorinated QLED was reduced from 3.5 to 2.5 V, and the roll-off current threshold was increased, resulting in a maximum brightness of 460,000 cd m^{-2} – a value two times higher than previously-reported LEDs employing solution-processed emitting layers. This strategy can be extended to QLEDs with different emission wavelengths to mitigate efficiency roll-off at high injection current densities and enable light sources with high brightness. It also takes a step in the direction of electrically-pumped CQD lasers[49].

Methods

Materials. Cadmium oxide (CdO, >99.99%), zinc acetate dihydrate ($Zn(AC)_2 \cdot 2H_2O$, 99.99%), sulfur powder (S, >99.5%), selenium powder (Se, >99.99%), oleylamine (OLA, 80-90%), octadecene (ODE, 90%), oleic acid (OA, 90%), tri-octylphosphine (TOP, 90%), thionyl chloride ($SOCl_2$), tetramethylammonium hydroxide (TMAH), 2-ethanolamine, tetrabutylammonium iodide (TBAI), tetrabutylammonium bromide (TBAB), tetrabutylammonium chloride (TBAC), as well as all kinds of solvents were purchased from Sigma Aldrich without further purification.

Synthesis of Zn-OLA complex. 2.45 g $Zn(AC)_2 \cdot 2H_2O$ was dissolved in 40 mL of OLA at 170 ^oC under vacuum to get a clear solution, and then cooled to room temperature and stored in air for use.

Preparation of CdSeZnS core-shell (C-S) and CdSeZnS-ZnS core-shell-shell (C-S-S) CQDs: The synthesis procedures of green-emitting C-S and C-S-S CQDs were referred to the literature with some modifications[29,32]. *For the synthesis of C-S CQDs*: 0.2 mmol of CdO and 4 mmol of $Zn(AC)_2$ were mixed with 5 mL of OA in a 100 mL flask and degassed for 30 min at 150 ^oC. 15 mL of ODE was injected into the reaction flask under N_2 and heated to 300 ^oC to get a clear solution of $Cd(OA)_2$ and $Zn(OA)_2$. 0.2 mmol of Se and 4 mmol of S dissolved in 2 mL of TOP was quickly injected into the flask at 300 ^oC. The reaction was kept at 300 ^oC for 10 min. *For the synthesis of C-S-S CQDs:* the temperature of above reaction solution was brought down to 290 ^oC, 1.5 mL as-prepared Zn-OLA diluted in 10.5 mL ODE was mixed with 0.03 g sulfur dissolved in 2 mL OLA, and then the mixture was injected into the flask at a speed of 14 mL hr^{-1} using a syringe pump to grow the ZnS shell. After finishing injection, the solution was annealed for 10 min at 290 ^oC, following by an injection of 4 mL OA. The products were purified by adding acetone, centrifugation at 6000 RPM and redispersing in toluene for 3 cycles.

Preparation of ZnO nanoparticles: Colloidal ZnO nanocrystals were synthesized by following a previous report with some modifications[4]. $Zn(AC)_2 \cdot 2H_2O$ (3 mmol) dissolved in 30 mL of DMSO solution was mixed with 10 ml of ethanol solution containing TMAH (5.5 mmol) and stirred for 24 h under ambient conditions. ZnO nanocrystals were then precipitated by adding ethyl acetate and centrifugation at 7000 RPM for 4 min. The precipitation was redispersed in ethanol and stored in the fridge, 160 µL of 2-ethanolamine was added to stabilize the solution. The ZnO nanocrystals were further washed with ethyl acetate and redispersed in ethanol, they are filtered before use.

Device Fabrication: ITO/glass substrates were ultrasonically cleaned with deionized water, acetone and 2-propanol for 60 min, respectively. ZnO nanoparticle solution was then spin-coated onto the ITO/glass substrates at 3000 rpm for 30 s and baked at 120 °C for 30 min. CQD dispersions in toluene (15 mg mL^{-1}) were spin-coated onto ZnO layer at 3000 rpm for 30s. The film was then soaked with the $SOCl_2$/acetonitrile solution for 30 s (volume ratio of $SOCl_2$ to acetonitrile is 1:1000, according to the calculation, the average amount of $SOCl_2$ on each CQDs is about 4.66×10^5, see details in Supporting Information), following by two times toluene rinse and subsequent baking at 120 °C for 30 min. CBP and MoO_x/Al electrodes were deposited using a thermal evaporation system through shadow masks under a high vacuum (<10^{-4} Pa). The active device areas were fixed as 3.14 mm^2. All devices were measured in the air without any encapsulation.

Commented [Z1]: Here is ACN or Toluene??

Material Characterization: Transmission electron microscopy (TEM) imaging was taken on JEOL 2010, with an acceleration voltage of 200 kV. PL spectra and decay dynamics data were collected on a Horiba Flurolog Time-Correlated Single Photon Counting (TCSPC) system, equipped with an iHR 320 monochromator and a PPO·900 detector. An Quanta-Phi integrating sphere was used for film and solution PLQY measurements. The morphology of film was measured using Scan Asyst on Bruker Catalyst in air. Fourier transform infrared spectroscopy (FT-IR) spectra were obtained from Nicolet 8700. XPS measurements were

performed using a Thermo Scientific K-Alpha system with electron-gun compensation to avoid sample charging and with 50 eV pass energy and binding energy step of 0.03–0.05 eV. The *J–L–V* characteristics of the QD-LEDs were measured under ambient conditions using an HP 4140B source meter. The absolute electroluminescence spectra were taken using an Ocean Optics USB4000 spectrometer that connected to a calibrated integrating sphere. An integration time of 10 ms was used for the USB4000 spectrometer to avoid saturation of CCD. The luminance values were calculated from the absolute EL spectra assuming a Lambertian distribution of the emission profile.

Optoelectronic Simulations: Calculations were carried out using the SCAPS 1D modeling suite[50]. Experimental bandgaps, band alignments, (imbalanced) mobilities, and active layer thicknesses were used (Table S6, Figure 3c). We note that asymmetries in the injection barriers and mobilities in the active layer can be canceled out by adjusting the workfunctions of the respective electrodes, resulting in nearly symmetric carrier distribution profiles. The analogous adjustments are also part of experimental device optimization. For a fair comparison, simulations with low and high mobilities were optimized independently in order to achieve the most symmetric carrier distribution and only then compared. Simulations results are presented at biases well past the flat-band condition but still at relatively low currents to maintain good numerical convergence. At higher injection currents, carrier imbalance and Auger recombination near the contacts will keep increasing.

Acknowledgements

This publication is based in part on work supported by Award KUS-11-009-21, made by King Abdullah University of Science and Technology (KAUST), by the Ontario Research Fund Research Excellence Program, and by the Natural Sciences and Engineering Research Council (NSERC) of Canada. The authors thank Bin Sun, Mengxia Liu, Marc Burgelman, Peng-Cheng Li, and Rahim Munir for their help during the course of study.

Author contributions

X.L. and F.F. conceived the idea. X.L. and F.F. developed the efficient chlorination exchange. X.L. and Y.Z. fabricated and characterized the QLEDs. O.V. performed optoelectronic device simulations. L.L. and X.L. synthesized the CQDs. M.L. did SEM imaging. R.Q.B. performed XPS characterization. X.L., F.F., O.V., E.H.S. and Y.B.Z. wrote the manuscript. O.V., E.H.S. and Z.H.L supervised the project. All authors discussed the results and assisted the manuscript preparation.

Additional information

The authors declare no competing financial interests. Correspondence and requests for materials should be addressed to ted.sargent@utoronto.ca, zhenghong.lu@utoronto.ca, o.voznyy@utornto.ca, and ffj@ustc.edu.cn.

Reference

1 Reineke, S. Complementary LED technologies. *Nat. Mater.* **14**, 459-462 (2015).

2 Shirasaki, Y., Supran, G. J., Bawendi, M. G. & Bulovic, V. Emergence of colloidal quantum-dot light-emitting technologies. *Nat. Photon.* **7**, 13-23 (2013).

3 Colvin, V. L., Schlamp, M. C. & Alivisatos, A. P. Light-emitting-diodes made from cadmium selenide nanocrystals and a semiconducting polymer. *Nature* **370**, 354-357 (1994).

4 Dai, X. *et al.* Solution-processed, high-performance light-emitting diodes based on quantum dots. *Nature* **515**, 96-99 (2014).

5 Cho, K.-S. *et al.* High-performance crosslinked colloidal quantum-dot light-emitting diodes. *Nat. Photon.* **3**, 341-345 (2009).

6 Qian, L., Zheng, Y., Xue, J. & Holloway, P. H. Stable and efficient quantum-dot light-emitting diodes based on solution-processed multilayer structures. *Nat. Photon.* **5**, 543-548 (2011).

7 Mashford, B. S. *et al.* High-efficiency quantum-dot light-emitting devices with enhanced charge injection. *Nat. Photon.* **7**, 407-412 (2013).

8 Dai, X., Deng, Y., Peng, X. & Jin, Y. Quantum-dot light-emitting diodes for large-area displays: Towards the dawn of commercialization. *Adv. Mater.* **29**, 1607022 (2017).

9 Shen, H. *et al.* High-efficiency, low turn-on voltage blue-violet quantum-dot-based light-emitting diodes. *Nano Lett.* **15**, 1211-1216 (2015).

10 Li, Z. *et al.* Efficient and long-life green light-emitting diodes comprising tridentate thiol capped quantum dots. *Laser Photon. Rev.* **11**, 1600227 (2017).

11 Coe, S., Woo, W.-K., Bawendi, M. & Bulovic, V. Electroluminescence from single monolayers of nanocrystals in molecular organic devices. *Nature* **420**, 800-803 (2002).

12 Yang, Y. *et al.* High-efficiency light-emitting devices based on quantum dots with tailored nanostructures. *Nat. Photon.* **9**, 259-266 (2015).

13 Shirasaki, Y., Supran, G. J., Tisdale, W. A. & Bulović, V. Origin of efficiency roll-off in colloidal quantum-dot light-emitting diodes. *Phys. Rev. Lett.* **110**, 217403 (2013).

14 Dolzhnikov, D. S. *et al.* Composition-matched molecular "solders" for semiconductors. *Science* **347**, 425-428 (2015).

15 Tang, J. *et al.* Colloidal-quantum-dot photovoltaics using atomic-ligand passivation. *Nat. Mater.* **10**, 765-771 (2011).

16 Chuang, C.-H. M., Brown, P. R., Bulović, V. & Bawendi, M. G. Improved performance and stability in quantum dot solar cells through band alignment engineering. *Nat. Mater.* **13**, 796-801 (2014).

17 Zhang, H., Jang, J., Liu, W. & Talapin, D. V. Colloidal nanocrystals with inorganic halide, pseudohalide, and halometallate ligands. *ACS Nano* **8**, 7359-7369 (2014).

18 Kovalenko, M. V., Scheele, M. & Talapin, D. V. Colloidal nanocrystals with molecular metal chalcogenide surface ligands. *Science* **324**, 1417-1420 (2009).

19 Choi, J. J. *et al.* Photogenerated exciton dissociation in highly coupled lead salt nanocrystal assemblies. *Nano Lett.* **10**, 1805-1811 (2010).

20 Sun, L. F. *et al.* Bright infrared quantum-dot light-emitting diodes through inter-dot spacing control. *Nat. Nanotech.* **7**, 369-373 (2012).

21 Lee, K.-H. *et al.* Over 40 cd/A efficient green quantum dot electroluminescent device comprising uniquely large-sized quantum dots. *ACS Nano* **8**, 4893-4901 (2014).

22 Owen, J. S., Park, J., Trudeau, P.-E. & Alivisatos, A. P. Reaction chemistry and ligand exchange at cadmium−selenide nanocrystal surfaces. *J. Am. Chem. Soc.* **130**, 12279-12281 (2008).

23 Zanella, M. *et al.* Atomic ligand passivation of colloidal nanocrystal films via their reaction with propyltrichlorosilane. *Chem. Mater.* **25**, 1423-1429 (2013).

24 Ji, C. *et al.* 1,2-Ethanedithiol treatment for $AgIn_5S_8$/ZnS quantum dot light-emitting diodes with high brightness. *ACS Appl. Mater. Interfaces* **9**, 8187-8193 (2017).

25 Daekyoung, K. *et al.* Improved electroluminescence of quantum dot light-emitting diodes enabled by a partial ligand exchange with benzenethiol. *Nanotechnology* **27**, 245203 (2016).

26 Pan, J. *et al.* Highly efficient perovskite-quantum-dot light-emitting diodes by surface engineering. *Adv. Mater.* **28**, 8718-8725 (2016).

27 Yang, Z. *et al.* All-quantum-dot infrared light-emitting diodes. *ACS Nano* **9**, 12327-12333 (2015).

28 Dirin, D. N. *et al.* Lead halide perovskites and other metal halide complexes as inorganic capping ligands for colloidal nanocrystals. *J. Am. Chem. Soc.* **136**, 6550-6553 (2014).

29 Bae, W. K. *et al.* Highly efficient green-light-emitting diodes based on CdSe@ZnS quantum dots with a chemical-composition gradient. *Adv. Mater.* **21**, 1690-1694 (2009).

30 Bae, W. K., Nam, M. K., Char, K. & Lee, S. Gram-scale one-pot synthesis of highly luminescent blue emitting $Cd_{1-x}Zn_xS$/ZnS nanocrystals. *Chem. Mater.* **20**, 5307-5313 (2008).

31 Lim, J. *et al.* Influence of shell thickness on the performance of light-emitting devices based on CdSe/$Zn_{1-X}Cd_XS$ Core/Shell heterostructured quantum dots. *Adv. Mater.* **26**, 8034-8040 (2014).

32 Adachi, M. M. *et al.* Microsecond-sustained lasing from colloidal quantum dot solids. *Nat. Commun.* **6**, 8694 (2015).

33 Lan, X. *et al.* Passivation using molecular halides increases quantum dot solar cell performance. *Adv. Mater.* **28**, 299-304 (2016).

34 Ning, Z. *et al.* Air-stable n-type colloidal quantum dot solids. *Nat. Mater.* **13**, 822-828 (2014).

35 Di Raddo, P. A convenient method of esterification of fatty acids: An undergraduate organic laboratory experiment. *J. Chem. Educ.* **70**, 1034 (1993).

36 Montalbetti, C. A. & Falque, V. Amide bond formation and peptide coupling. *Tetrahedron* **61**, 10827-10852 (2005).

37 Bae, W. K. *et al.* Highly effective surface passivation of PbSe quantum dots through reaction with molecular chlorine. *J. Am. Chem. Soc.* **134**, 20160-20168 (2012).

38 Bae, W. K. *et al.* Controlling the influence of Auger recombination on the performance of quantum-dot light-emitting diodes. *Nat. Commun.* **4**, 2661 (2013).

39 Blakesley, J. C. *et al.* Towards reliable charge-mobility benchmark measurements for organic semiconductors. *Org. Electron.* **15**, 1263-1272 (2014).

40 Baranovski, S. *Charge Transport in Disordered Solids with Applications in Electronics*. Vol. 17 (John Wiley & Sons, 2006).

41 Talgorn, E. *et al.* Unity quantum yield of photogenerated charges and band-like transport in quantum-dot solids. *Nat. Nanotech.* **6**, 733-739 (2011).

42 Jasieniak, J., Califano, M. & Watkins, S. E. Size-dependent valence and conduction band-edge energies of semiconductor nanocrystals. *ACS Nano* **5**, 5888-5902 (2011).

43 Kwak, J. *et al.* Bright and efficient full-color colloidal quantum dot light-emitting diodes using an inverted device structure. *Nano Lett.* **12**, 2362-2366 (2012).

44 Pan, J. *et al.* Size tunable zno nanoparticles to enhance electron injection in solution processed QLEDs. *ACS Photonics* **3**, 215-222 (2016).

45 Helander, M. G. *et al.* Chlorinated indium tin oxide electrodes with high work function for organic device compatibility. *Science* **332**, 944-947 (2011).

46 Piprek, J., Romer, F. & Witzigmann, B. On the uncertainty of the Auger recombination coefficient extracted from InGaN/GaN light-emitting diode efficiency droop measurements. *Appl. Phys. Lett.* **106**, 101101 (2015).

47 Bae, W. K. *et al.* Controlled alloying of the core–shell interface in CdSe/CdS quantum dots for suppression of Auger recombination. *ACS Nano* **7**, 3411-3419 (2013).

48 Dong, Y. *et al.* 20.2: Ultra-bright, highly efficient, low roll-off inverted quantum-dot light emitting devices (QLEDs). *SID Symposium Digest of Technical Papers* **46**, 270-273 (2015).

49 Fan, F. *et al.* Continuous-wave lasing in colloidal quantum dot solids enabled by facet-selective epitaxy. *Nature* **544**, 75-79 (2017).

50 Burgelman, M., Decock, K., Khelifi, S. & Abass, A. Advanced electrical simulation of thin film solar cells. *Thin Solid Films* **535**, 296-301 (2013).

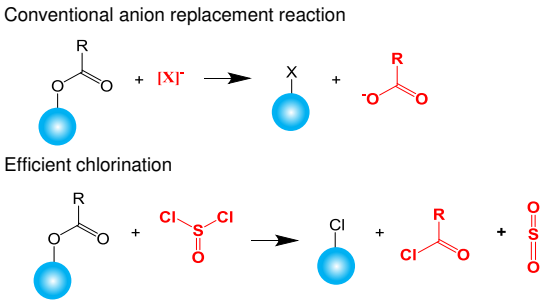

Figure 1. Chlorination ligand exchange mechanism. Chemical equations for conventional anion replacement and efficient chlorination processes. X stands for halides, pseudo-halides, sulfides, metal complexes, etc.

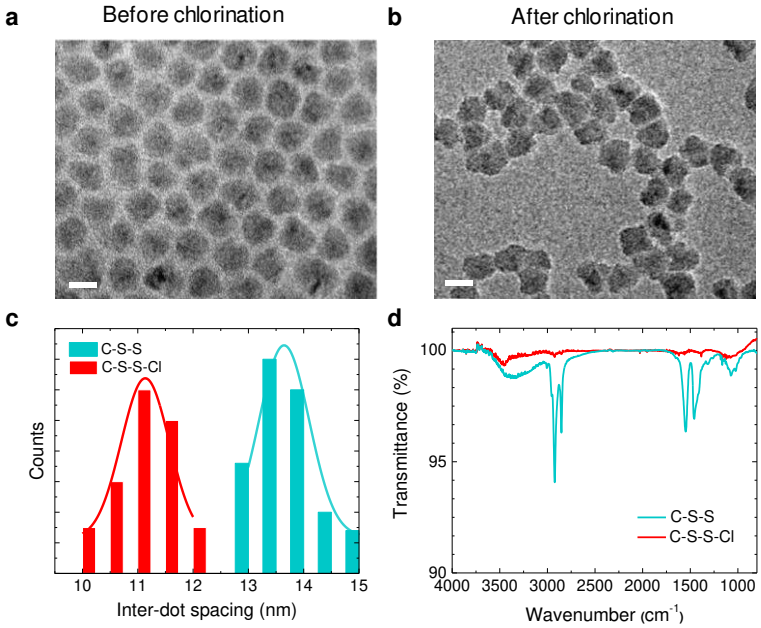

Figure 2. Characterization of C-S-S CQD after chloride exchange (C-S-S-Cl CQD). (a) and (b) TEM images of C-S-S and C-S-S-Cl CQDs. Scale bar: 10 nm. (c) Histograms of the inter-dot spacing extracted from (a) and (b). (d) FTIR spectra of CQD films showing the removal of organic ligands upon efficient chlorination.

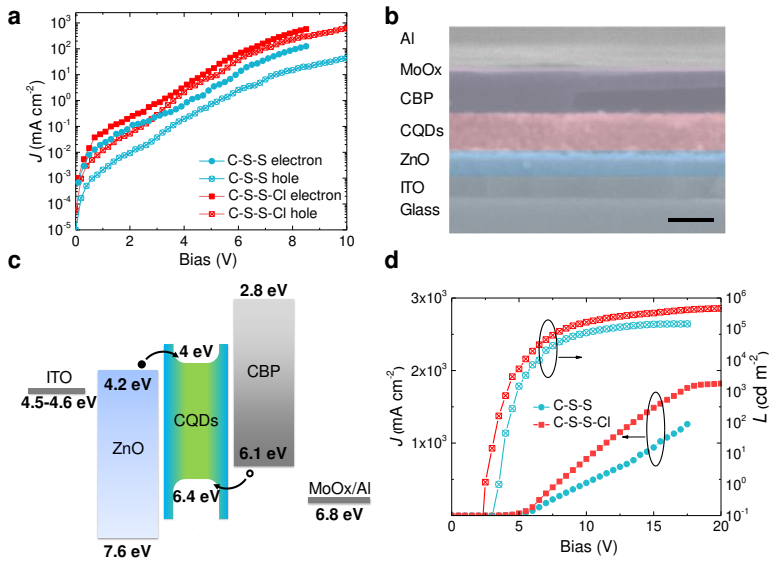

Figure 3. Conductivity and QLED architecture. Ccharacterization ~~and QLED architectureof QLEDs devices~~. (a) Current density-bias (*J*–*V*) characteristics of electron- and hole-only devices based on C-S-S and C-S-S-Cl CQDs. (b) Cross-sectional SEM image (scale bar: 60 nm), and (c) energy diagram of different layers of C-S-S-Cl QLED. (d) Current density–luminance–bias (*J*–*L*–*V*) characteristics of the C-S-S and C-S-S-Cl QLEDs, respectively.

Formatted: Font: Bold

Formatted: Font: Bold

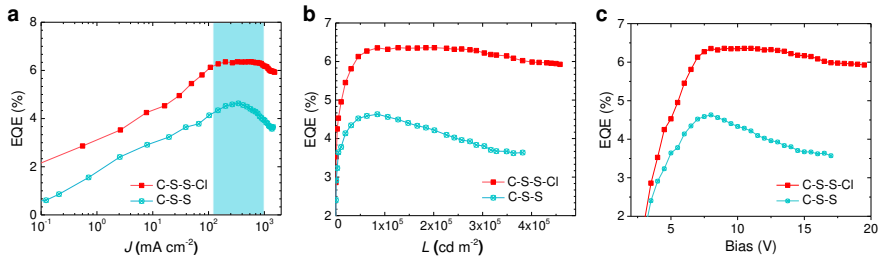

Figure 4. EQE Ccharacterization of QLED~~s~~ devices. EQE as a function of (a) current density, (b) luminance, and (c) bias of the C-S-S and C-S-S-Cl QLEDs, respectively.~~s.~~

Formatted: Font: Bold

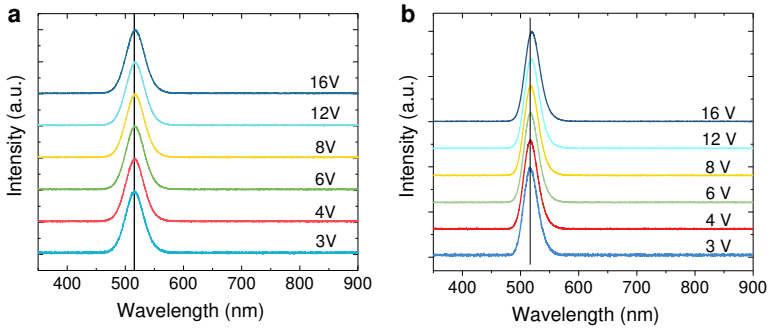

Figure 5. Electroluminescence ~~luminescence~~spectra under different biases. ~~for~~ (a) C-S-S-Cl and (b) C-S-S QLEDs devices, respectively.

Formatted: Font: Not Bold

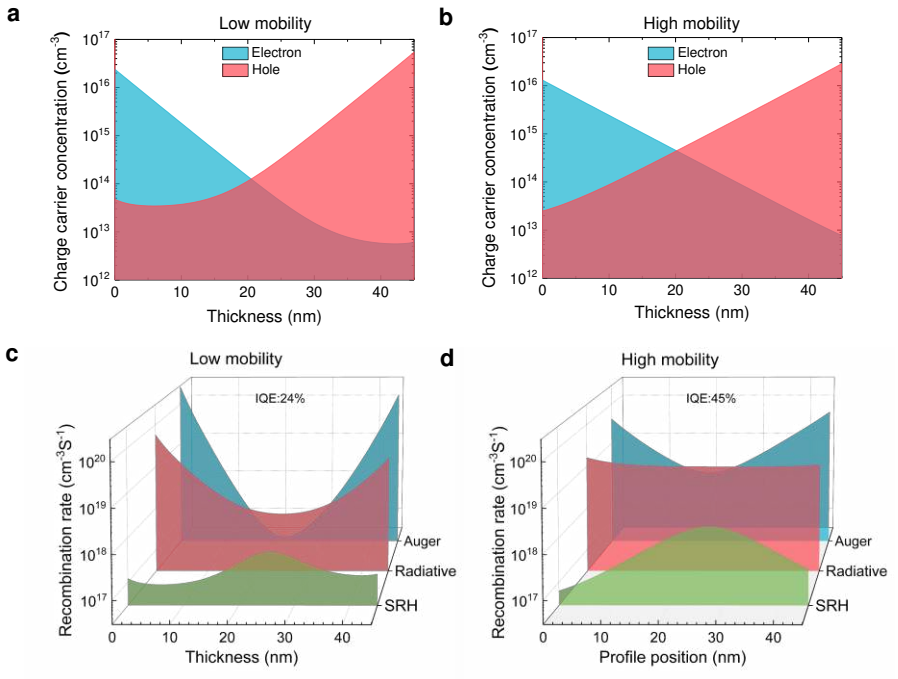

Figure 6. Optoelectronic simulations of charge carrier distributions and recombination rates inside the active layers. The charge carrier distribution inside the 45 nm thick CQD active layers with low (a) and high (b) mobilities, respectively, at an equivalent injection

current in a QLED. The corresponding recombination rates and the resultant internal quantum efficiency (IQE) (c) and (d) (note the logarithmic scale). SRH denotes nonradiative Shockley-Read-Hall recombination through trap states.